**J. Cent. South Univ.** (2013) 20: 799−811
**DOI:** 10.1007/s11771-013-1551-6

Springer

# Effects of axial cyclic loading at constant confining pressures on deformational characteristics of anisotropic argillite

ZHANG Jiu-chang(张久长)[1], ZHOU Su-hua(周苏华)[2], FANG Li-gang(方理刚)[2], XU Xiang-hua(许湘华)[3]

1. Institute of Geotechnical Engineering, Hohai University, Nanjing 210098, China;
2. School of Civil Engineering, Central South University, Changsha 410075, China;
3. Guizhou Provincial Department of Transportation, Guiyang 550003, China



**Abstract:** Triaxial cyclic loading tests have been performed to assess the influence of plastic deformation on inelastic deformational properties of anisotropic argillite with bedding planes which is regarded as a kind of transversely isotropic media. Considering argillite's anisotropy and inelastic deformational properties, theoretical formulae for calculating oriented elastic parameters were deduced by the unloading curves, which can be better fitted for the description of its elasticity than loading curves. Test results indicate that with the growth of accumulated plastic, strain, the apparent elastic modulus of argillite decreases in a form of exponential decay function, whereas the apparent Poisson ratio increase in a form of power equation. A ratio of unloading recoverable strain to the total strain increment occurred during a loading cycle is defined to illustrate the characteristic relations between anisotropic coupled elasto-plastic deformation and plastic strain. It is significant to observe that high stress level and plastic history have an inhibiting effect on argillite anisotropy.

**Key words:** anisotropic argillite; coupled elasto-plasticity; cyclic loading tests; elastic parameters; plastic strain

## 1 Introduction

Experimental investigations reveal that rocks are anisotropic in deformation and strength, especially those rocks with fabric elements in the form of bedding, foliation, layering, fissuring, stratification or jointing [1−4]. Moreover, many theoretical and experimental studies show that elastic parameters of rock-like materials vary as plastic deformation occurs, which is known as inelasticity [5] and coupled elasto-plastic deformation [6−10]. Therefore, it is reasonable to consider that anisotropy and coupled elasto-plasticity are the two principal characteristics of bedding rocks, which are often mechanically regarded as transversely isotropic media. However, interactions and relations between both these characteristics are seldom covered by recent studies on elasto-plasticity of anisotropic rocks. Generally, the anisotropy and coupled elasto-plasticity of rock are researched individually.

As for the anisotropy of rock, several methodologies [1−2, 4, 11−13] for determining elastic parameters have been proposed, which are basically meaningful for further studies on this issue. Certainly, more important researches have been done, such as anisotropic failure criteria [14−19], elasto-plastic models [20] and even more sophisticated coupled elasto-plastic damage model [21−24]. These works provide more accurate prediction for complex physical phenomena of anisotropic rocks, like failure and plasticity.

As far as coupled elasto-plasticity is concerned, theories and experiments were mainly focused on isotropic media [6−10, 25]. Theoretically, based upon the first and second laws of thermodynamics and Iliushins' postulate in strain space, DAFALIAS [8−9] pointed out that non-associated flow occurs when materials exhibit coupled elasto-plastic deformation in his ground-breaking research. On the second law of thermodynamics, internal friction force brings about heat dissipation, which means that entropy irreversibly increases and results in non-associated flow [8−10]. This principle illustrates that plastic evolution inevitably affects the properties of materials. More practically, BIGONI and HUECKEL [6−7] discussed some issues on uniqueness and localization related to coupled elasto-plasticity and non-associated flow, respectively. MAIER and

**Foundation item:** Program(2011CB710601) supported by National Basic Research Program of China; Project(50925933) supported by National Natural Science Foundation of China; Project(2008BAB29B03) supported by National Key Technology Research and Development Program of China; Project(2010-122-011) supported by Guizhou Provincial Department of Transportation, China
**Received date:** 2011−12−30; **Accepted date:** 2012−03−13
**Corresponding author:** FANG Li-gang, Professor; Tel: +86−731−82539756; E-mail: fangligangcsu@163.com

HUECKEL [10] established a constitutive model which incorporated an elasto-plastic coupled strain. These researches theoretically provide a solid and necessary support for further studies.

Experimentally, uniaxial and triaxial cyclic loading tests controlled by servo-mechanical testing system are the best choice for studying the coupled elasto-plastic issue. Under consolidated-undrained triaxial cyclic loading conditions, YOSHINAKA et al [26−27] studied mechanical properties of four saturated Miocene soft rocks in Japan, and a significant finding is that the elastic modulus of rock decreases with the increases of plastic strain according to exponential equations.

Recently, FUENKAJORN and PHUEAKPHUM [28] studied the influences of uniaxial cyclic loading on instantaneous and long-term creep properties of Maha Sarakham salt. Furthermore, in the view of microcracking, with two types of uniaxial cyclic loading test schemes, such as increasing-amplitude cyclic loading and constant-amplitude cyclic loading, HEAP and FAULKNER [29] researched the evolution features of static elastic properties of a kind of small-grain-sized Westerly granite. More significantly, similar experimental results have been observed by ZHANG et al [30], when they studied coupled elasto-plasticity of a kind of marble in both deformation and strength. All of these researches are discussed on isotropic rocks.

To anisotropic ones, less attentions of coupled elsto-plasticity are paid. NIANDOU et al [31] conducted triaxial compression cyclic tests to study the properties of Tournemire shale in France (this shale is of transverse isotropy). The excellent relations they obtained were a series of empirical functions between the shale's five elastic parameters and confining pressures. Although there was an evident phenomenon of coupled elasto-plasticity exhibiting in their stress−strain hysteresis curves of triaxial cyclic tests, no further research was discussed on this issue to establish relations between anisotropy and coupled elasto-plastic deformation.

In this work, a detailed study on both anisotropy and coupled elasto-plasticity of anisotropic argillite was presented. Firstly, with basic rules of coupled elasto-plasticity, formulae for calculating elastic, plastic and coupled elasto-plastic strains, as well as equations that define elastic parameters by using cyclic unloading curves were proposed. Then, elastic theory and related five elastic parameters of transversely isotropic rocks were recapitulated. Based on the previous researches, relations between apparent elastic modulus (as well as apparent Poisson ratio) and plastic internal variable for transversely isotropic rocks were suggested. Secondly, triaxial loading cyclic tests on argillite specimens with various loading angles at two confining pressures were conducted. By analyzing test data, argillite's characteristics of transversely isotropic coupled elasto-plasticity were studied. Finally, empirical functions between five elastic parameters and axial plastic strain (taken as plastic internal variable) were acquired.

## 2 Coupled elasto-plastic deformation of rocks

### 2.1 Elastic, plastic and coupled elasto-plastic strains

Cyclic loading stress−strain curves of a rock specimen (whether this rock is isotropic or not) are illustrated in Fig. 1, where linear segments $OA$ and $OP$ are the axial and radial stress−strain curves, with their slopes $E^{\circ}$ and $-\nu^{\circ}/E^{\circ}$, respectively. $E^{\circ}$ is defined as the original elastic modulus and $\nu^{\circ}$ the original Poisson ratio when no plastic strains occur. Passing point $A$ or $P$, the total strain of rock specimen will contain plastic part. For the purpose of making distinctions among various loading cycles, $A_i$ and $P_i$ are the $i$-th unloading points.

For those ideal materials, unloading from point $A_i$ or $P_i$, the stress−strain curve will pass along the curve $A_iH_i$ or $P_iH_i$, parallel to $OA$ or $OP$. Curves of unloading and subsequent re-loading are overlapped. Point $H_i$ or $V_i$ is the endpoint of unloading, and also the start point of re-loading. For such ideal conditions, $A_iH_i//OA$ and $P_iV_i//OP$, coupled elasto-plastic deformation does not exist.

Generally, rock materials show different behaviors. However, from point $A_i$ or $P_i$ the stress unloads to point $C_i$ or $R_i$ on the real unloading path $A_iB_iC_i$ or $P_iQ_iR_i$, then it re-loads along curve $C_iD_iE_iA_{i+1}$ or $R_iS_iT_iP_{i+1}$. Due to the non-coincidence between unloading and re-loading curves, a stress−strain hysteresis loop $A_iB_iC_iD_iE_i$ or $P_iQ_iR_iS_iT_i$ is formed. Point $C_i$ or $R_i$ is the nadir of hysteresis loop, and point $E_i$ or $T_i$ the vertex.

Actually, point $C_i$ or $R_i$ is the endpoint of unloading and does not always coincide with the ideal unloading endpoint $H_i$ or $V_i$, because it invariably falls in front of $H_i$ or $V_i$. This phenomenon is called coupled elasto-plastic deformation, which has been discussed in many literatures [8−10, 25−27]. At the unloading point $A_i$ or $P_i$, the total strain thus can be divided into irreversible plastic and reversible parts as

$$OF_i = C_iF_i + OC_i \quad \text{viz} \quad \varepsilon_{\mathrm{a}}^{(i)} = \varepsilon_{\mathrm{a}}^{\mathrm{r}(i)} + \varepsilon_{\mathrm{a}}^{\mathrm{p}(i)} \tag{1}$$

$$OU_i = R_iU_i + OR_i \quad \text{viz} \quad \varepsilon_{\mathrm{r}}^{(i)} = \varepsilon_{\mathrm{r}}^{\mathrm{r}(i)} + \varepsilon_{\mathrm{r}}^{\mathrm{p}(i)} \tag{2}$$

Equations (1) and (2) are respectively for axial and

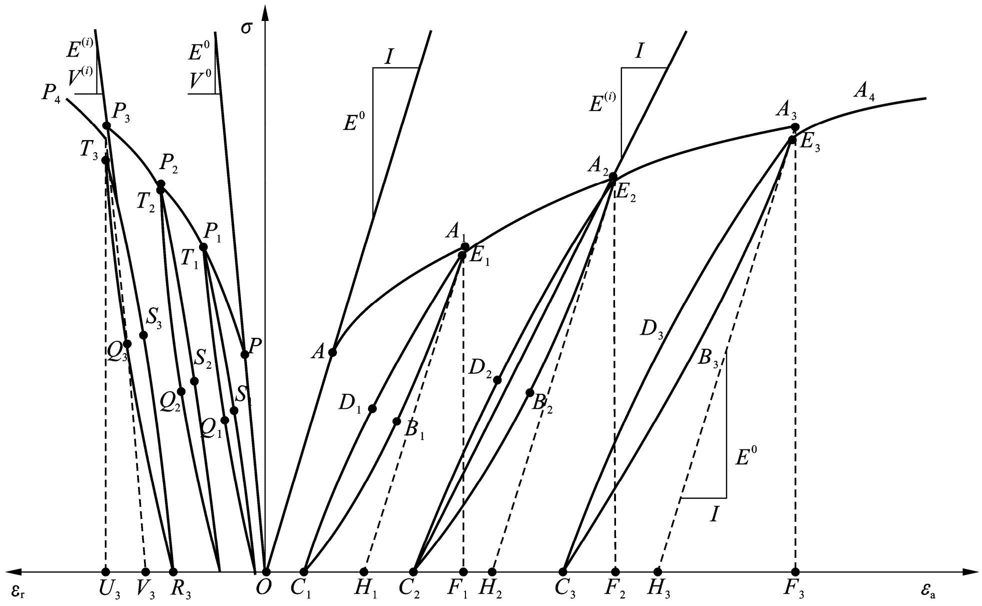


**Fig. 1** Illustration of coupled elasto-plastic stress-strain curves of a rock specimen under uniaxial cyclic loading

radial strain relations. Subscript "a" stands for "axial", and "r" for "radial". Superscript " ($i$) " stands for unloading cycles, as well as "r' and "p" stand for "reversible" and "plastic" strains, respectively. The total strains ($\varepsilon_{\mathrm{a}}^{(i)}$ and $\varepsilon_{\mathrm{r}}^{(i)}$) and plastic strains ($\varepsilon_{\mathrm{a}}^{\mathrm{p}(i)}$ and $\varepsilon_{\mathrm{r}}^{\mathrm{p}(i)}$) can be measured by testing.

The strain $H_iF_i$ or $V_iU_i$ rebounding along the ideal unloading curve is defined as elastic strain $\varepsilon_{\mathrm{a}}^{\mathrm{e}(i)}$ (or $\varepsilon_{\mathrm{r}}^{\mathrm{e}(i)}$). While the strain $C_iF_i$ or $R_iU_i$ rebounding along the real unloading curve $A_iB_iC_i$ (or $R_iQ_iR_i$) is defined as the resilient strain $\varepsilon_{\mathrm{a}}^{\mathrm{r}(i)}$ (or $\varepsilon_{\mathrm{r}}^{\mathrm{r}(i)}$). Thus, the resilient strain includes a part of strain $C_iH_i$ or $R_iV_i$ that is called coupled elasto-plastic strain $\varepsilon_{\mathrm{a}}^{\mathrm{ep}(i)}$ ($\varepsilon_{\mathrm{r}}^{\mathrm{ep}(i)}$). So, the total strain can be divided into three parts, which are

$$\varepsilon_{\mathrm{a}}^{(i)}=\varepsilon_{\mathrm{a}}^{\mathrm{e}(i)}+\varepsilon_{\mathrm{a}}^{\mathrm{ep}(i)}+\varepsilon_{\mathrm{a}}^{\mathrm{p}(i)} \tag{3}$$

$$\varepsilon_{\mathrm{r}}^{(i)}=\varepsilon_{\mathrm{r}}^{\mathrm{e}(i)}+\varepsilon_{\mathrm{r}}^{\mathrm{ep}(i)}+\varepsilon_{\mathrm{r}}^{\mathrm{p}(i)} \tag{4}$$

### 2.2 Elastic parameters defined by unloading curves

Rocks are porous materials with numerous micro-pores and micro-cracks. When they are applied with compressive stress, they (especially soft rocks) will exhibit irreversible plastic deformation. Many cyclic loading tests show that rocks inevitably develop new plastic strains during the process of loading. Thus, the deformational parameters tested by loading curves are exactly those of elasto-plasticity [32].

Therefore, elastic parameters determined by unloading curves are much more proper and truly able to reflect elasticity of rocks than those tested by loading curves. In this work, a testing method, defined on the unloading curves of triaxial cyclic tests, is suggested and adopted to calculate the argillite elastic parameters. As shown in Fig. 1, we connect the unloading point $A_i$ and the nadir $C_i$ of hysteresis loop with a line segment $A_iC_i$. So, the average elastic modulus $E^{(i)}$ of $A_iB_iC_i$ at the $i$-th unloading cycle can be represented by

$$E^{(i)}=\frac{F_iA_i}{C_iF_i}=\frac{\sigma(i)}{\varepsilon_{\mathrm{a}}^{\mathrm{r}(i)}} \tag{5}$$

where $\sigma^{(i)}$ is the stress at the unloading point $A_i$ and $E^{(i)}$ equals the slope of $A_iC_i$. Precisely the same with modulus, we have following formula to define Poisson ratio $\nu^{(i)}$

$$\nu^{(i)}=-\frac{R_iU_i}{C_iF_i}=-\frac{\varepsilon_{\mathrm{r}}^{\mathrm{r}(i)}}{\varepsilon_{\mathrm{a}}^{\mathrm{r}(i)}} \tag{6}$$

In Eqs. (3) and (4), elastic strains ($\varepsilon_{\mathrm{a}}^{\mathrm{e}(i)}$ and $\varepsilon_{\mathrm{r}}^{\mathrm{e}(i)}$) and coupled elasto-plastic strains ($\varepsilon_{\mathrm{a}}^{\mathrm{ep}(i)}$ and $\varepsilon_{\mathrm{r}}^{\mathrm{ep}(i)}$) can be calculated by Eqs. (7) and (8):

$$\varepsilon_{\mathrm{a}}^{\mathrm{e}(i)}=\frac{\sigma^{(i)}}{E^0},\ \varepsilon_{\mathrm{a}}^{\mathrm{e}(i)}=\frac{\nu^0}{E^0}\sigma^{(i)} \tag{7}$$

$$\begin{cases}\varepsilon_{\mathrm{a}}^{\mathrm{e}(i)}=\dfrac{(E^0-E^{(i)})\sigma^{(i)}}{E^0E^{(i)}}\\[2ex] \varepsilon_{\mathrm{r}}^{\mathrm{ep}(i)}=\left(\dfrac{\nu^0}{E^0}-\dfrac{\nu^{(i)}}{E^{(i)}}\right)\sigma^{(i)}\end{cases} \tag{8}$$

## 3 Triaxial cyclic loading tests

### 3.1 Elastic parameters of bedding rocks

Rock with one regular bedding plane or foliation can be simplified as transversely isotropic material. This indicates that at each point in the rock there is an axis of rotational symmetry and that the rock has isotropic properties in the plane normal to that axis, this plane being the plane of transverse isotropy [1].

Figure 2 shows the uniaxial compression test of a transversely isotropic rock specimen with an angle of $\beta$, which is both the sampling angle and the loading angle. $\beta$ is also the angle between axis of rock specimen and its isotropic plane. $\beta_z$ is the applied compression stress on the end of specimen.

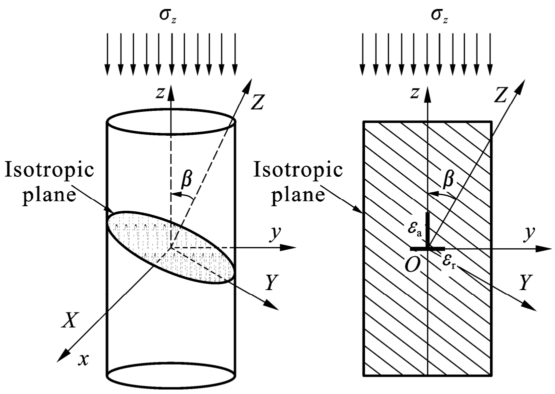


**Fig. 2** Specimen illustration of transversely isotropic rocks

In Fig. 2, a fabric coordinate system *OXYZ* attached to the structure is set up, with its *Z*-fold axis being the axis of rotational symmetry and *XOY* plan being the plane of transverse isotropy. The global coordinate system $O_{xyz}$ is obtained by rotating *OXYZ* counterclockwise around the *X*-axis with an angle of $\beta$. Transversely isotropic materials have five elastic parameters, with the following definitions [1]: $E_1$ and $E_2$ are elastic moduli in the plane of transverse isotropy and in the direction normal to it, respectively; $\nu_1$ and $\nu_2$ are Poisson ratios characterizing the lateral strain response in the plane of transverse isotropy to a stress acting parallel or normal to it, respectively; $G_2$ is the shear modulus in planes normal to the plane of transverse isotropy.

Some methodologies were developed by using uniaxial [1−3] and triaxial tests [11, 31] to determine the five elastic parameters. It is assumed that theories and formulae deduced for isotropic rocks are suitable for anisotropic rocks. So, as for the transversely isotropic rocks, their five elastic parameters and the plastic internal variable are supposed to be abstractly related as

$$\begin{cases} E_1 = E_1(\xi), \quad \nu_1 = \nu_1(\xi) \\ E_2 = E_2(\xi), \quad \nu_2 = \nu_2(\xi) \\ G_2 = G_2(\xi) \end{cases} \tag{9}$$

where $\xi$ is the plastic internal variable. Moreover, the apparent elastic modulus $E_\beta$ and apparent Poisson ratio $\nu_\beta$ vary with loading angle $\beta$ as well, so we suppose

$$E_\beta = E_\beta(\xi, \beta) \tag{10}$$

$$\nu_\beta = \nu_\beta(\xi, \beta) \tag{11}$$

### 3.2 Rock specimen preparation

The argillite rock specimens were sampled from an excavation slope in Sige Service Area of Xiamen-Chengdu Expressway in Rongjiang County, Guizhou Province, China (Fig. 3). Specimens were cored by a drilling at different angles $\beta$ (0°, 15°, 30°, 45°, 60° and 90°) and cut from the core samples with a saw machine. Then, the ends of specimens were made flat with a grinding machine. All specimens were about 42 mm in diameter and 99 mm in length (Fig. 4). Their physical and geometrical parameters are listed in Table 1.

BX120-5AA foil strain gauges were glued in the way shown in Fig. 2. The angles of strain gauges were 0° and 90°, which can be used for testing radial strain $\varepsilon_r$ and axial strain $\varepsilon_a$ of a rock specimen.

### 3.3 Triaxial cyclic loading tests

Instron 1346 Servo-controlled Mechanical Testing System was used for all triaxial cyclic loading tests in this work. The system consists of a confining pressure cell, a data acquisition instrument, load frame, test controller and a computer. Loading, unloading and data collection can be conducted under the control of system software.

The argillite rock specimens were wrapped in a rubber membrane and put into the sealed triaxial cell. By starting the system, confining pressure was firstly and gradually applied and reached the pre-set value. But the axial force was applied at the tempo of 0.2 kN/s. The frequency of collecting data by an instrument was set as 1 Hz, namely one time each second. During a test, the confining pressure was kept as constant and cross-section compression stress of specimen was taken as traxial cyclic loading control points (listed in Table 2). When one specimen's cross-section compression stress unloaded to its confining pressure, unloading was stopped. The rate of unloading was the same as that of loading.

### 3.4 Test results

Stress−strain curves for triaxial cyclic loading tests of argillite rock specimens with different coring angles are graphed in Figs. 5 and 6 at confining pressures of 5 MPa and 10 MPa, respectively. Due to the failure of system's data cable in the connection between foil strain gauges and triaxial cell, the radial strain data of rock

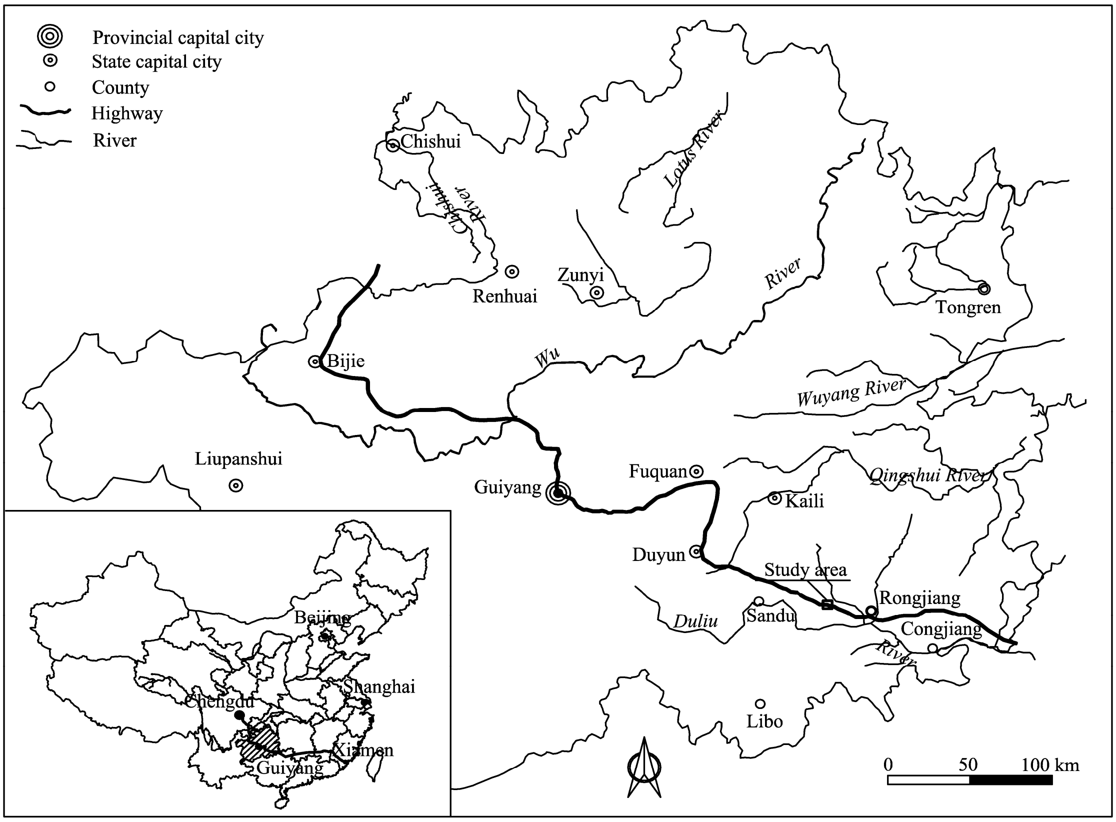


**Fig. 3** Location of investigation site in Guizhou Province, China

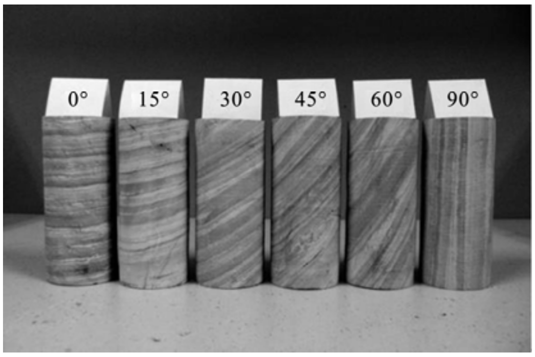


**Fig. 4** Tested anisotropic argillite specimens with various coring angles

specimens when angle $\beta$ was 15°, 30° and 60° were not recorded.

## 4 Relations between elastic parameters and plastic axial strain

In terms of plasticity of geo-materials, plastic work and plastic strain are often chosen as plastic internal variables. Following this convention, axial plastic strain $\varepsilon_a^p$ is adopted as plastic internal variable to substitute $\xi$ in the following context. So, we assume that $E_\beta$ and $\nu_\beta$ are the common functions of axial plastic strain $\varepsilon_a^p$ and loading angle $\beta$.

**Table 1** Physical and geometrical parameters of specimens

| Confining pressure/ MPa | Dip of bedding/ (°) | Dimensions/mm | | Length/ Diameter ratio | Density/ (kg·m$^{-3}$) |
|---|---|---|---|---|---|
| | | Length | Diameter | | |
| 5 | 0 | 99.50 | 42.23 | 2.36 | 2 617.99 |
| 5 | 15 | 99.67 | 42.51 | 2.34 | 2 559.23 |
| 5 | 30 | 97.74 | 42.43 | 2.30 | 2 498.16 |
| 5 | 45 | 98.44 | 42.22 | 2.33 | 2 478.74 |
| 5 | 60 | 98.55 | 42.38 | 2.33 | 2 447.98 |
| 5 | 90 | 96.18 | 42.17 | 2.28 | 2 423.45 |
| 10 | 0 | 99.74 | 42.65 | 2.34 | 2 593.49 |
| 10 | 15 | 99.83 | 42.25 | 2.36 | 2 516.91 |
| 10 | 30 | 99.01 | 42.44 | 2.33 | 2 517.55 |
| 10 | 45 | 98.72 | 42.36 | 2.33 | 2 518.35 |
| 10 | 60 | 98.50 | 42.35 | 2.33 | 2 429.21 |
| 10 | 90 | 101.39 | 42.40 | 2.39 | 2 449.12 |

**Table 2** Unloading control points for triaxial cyclic loading, $\sigma$, $\sigma_1$/MPa

| Loading cycle | $\sigma_3$=5 MPa | $\sigma_3$=10 MPa |
|---|---|---|
| 1 | 10 | 15 |
| 2 | 15 | 20 |
| 3 | 20 | 25 |
| 4 | 25 | 30 |
| 5 | 30 | 35 |
| 6 | 35 | 40 |
| 7 | 40 | 45 |

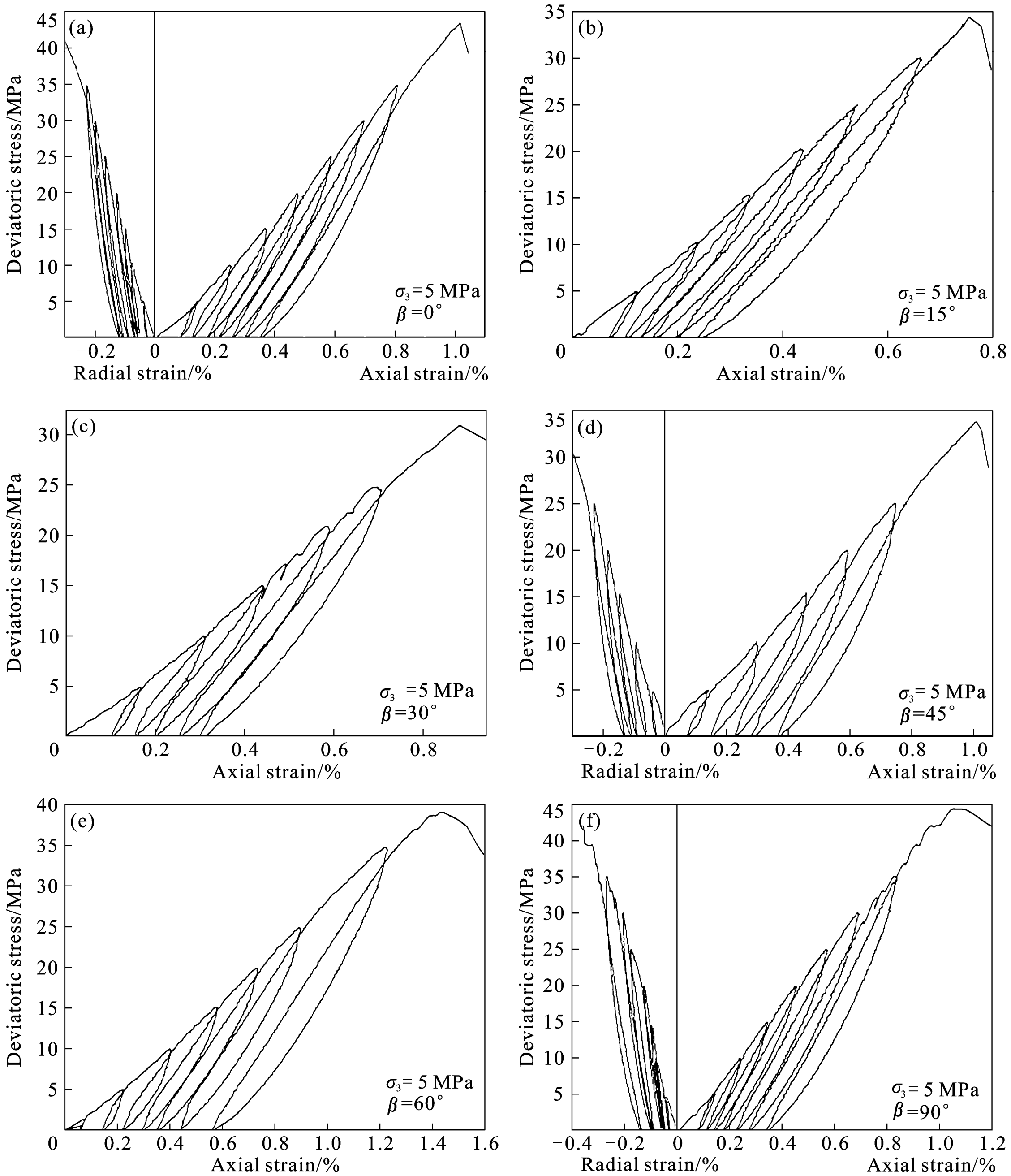


**Fig. 5** Triaxial cyclic loading stress-strain curves of argillite specimens with different dip angles (confining pressure: 5 MPa)

### 4.1 Variations of oriented elastic parameters

Apparent elastic modulus $E_\beta$ and axial plastic strain $\varepsilon_a^p$ corresponding to different unloading cycles can be calculated with Eq. (5) and measured by tests, respectively. A significant finding in this work is that apparent elastic modulus of argillite decreases with the growth of axial plastic strain and eventually is close to a constant. This characteristic of argillite can be illustrated with an exponential decay function:

$$E_\beta = B + A\exp\left(\frac{\varepsilon_a^p}{t}\right) \tag{12}$$

where $B$, $A$ and $t$ are empirical parameters and related to loading angle $\beta$. Figure 7 shows experimental values and data-fitting curves of $E_\beta$ vs $\varepsilon_a^p$ at various loading angles and under two confining pressures. By data-fitting with Eq. (12), $B$, $A$ and $t$ corresponding to loading angles can be obtained and listed in Table 3.

While $\beta$ is confined to be a constant and a series of $\varepsilon_a^p$ is substituted into Eq. (12), a series of changing $E_\beta$ corresponding to this fixed $\beta$ will be obtained. By linking these points of $E_\beta$ with same values of $\varepsilon_a^p$, curves between $E_\beta$ and $\beta$ can be graphed in Fig. 8. These curves are called contour curves of $E_\beta$ vs $\beta$ at equivalent $\varepsilon_a^p$. From Fig. 8, it is interesting to draw the following results:

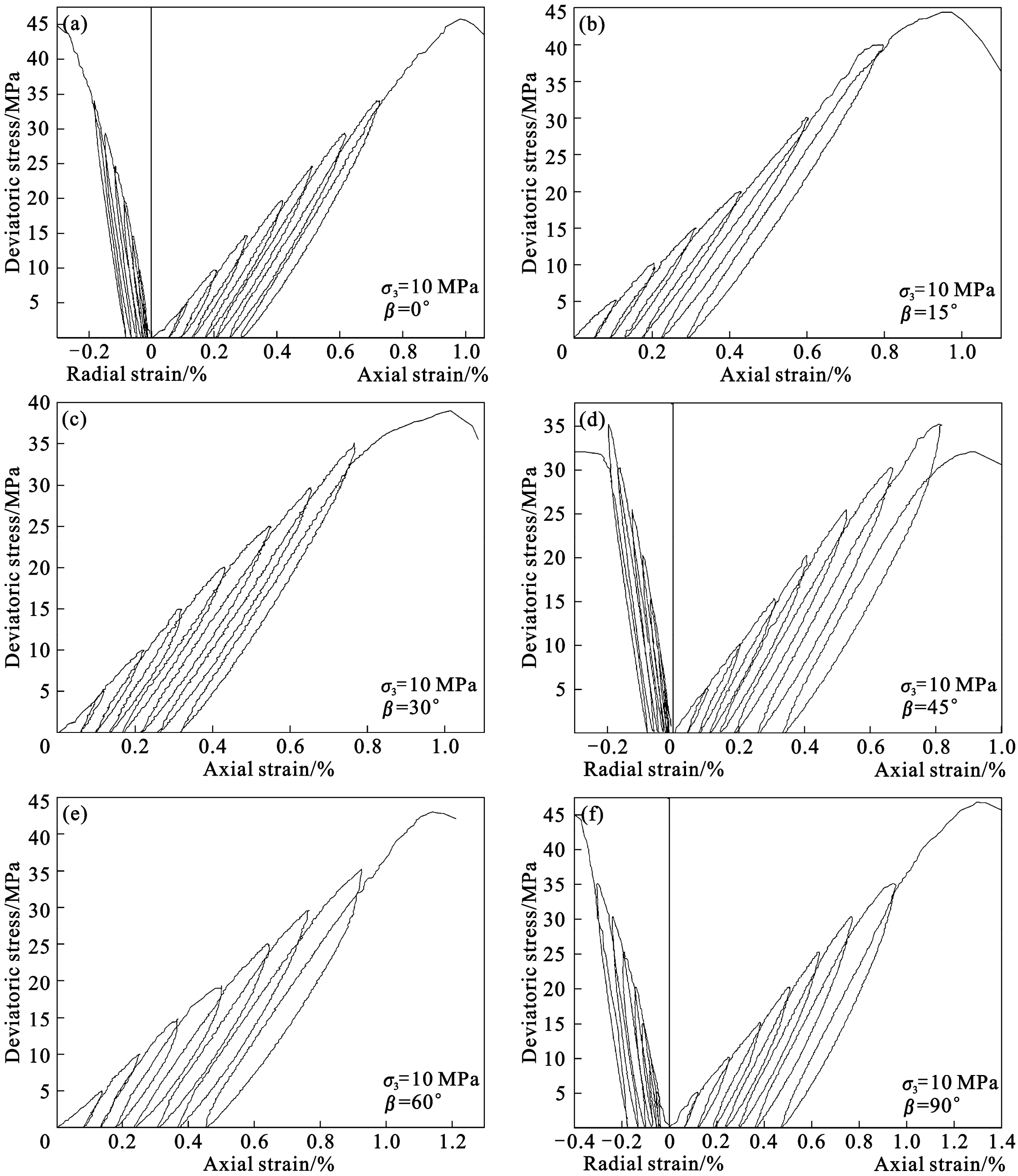


**Fig. 6** Triaxial cyclic loading stress-strain curves of argillite specimens with different dip angles (confining pressure: 10 MPa)

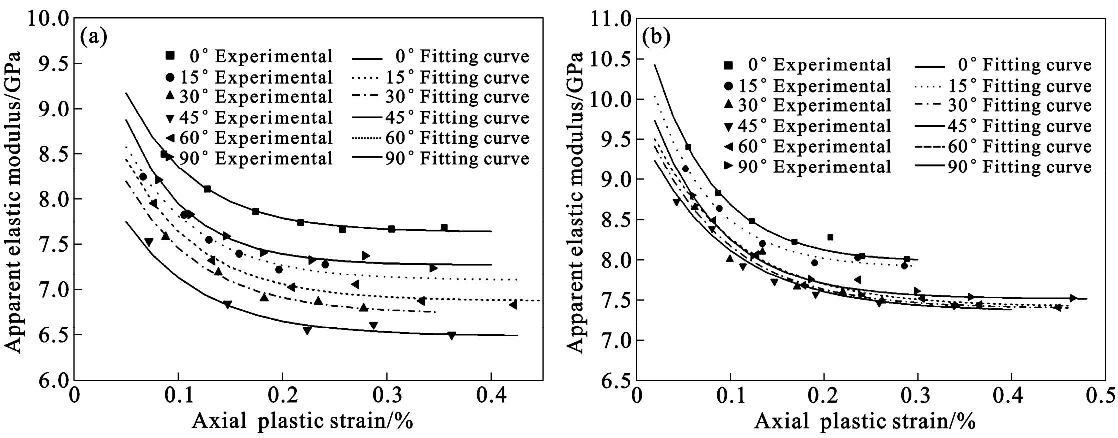


**Fig. 7** Relationships between apparent elastic modulus and axial plastic strain at two confining pressures: (a) 5 MPa; (b) 10 MPa

**Table 3** Values of parameters $A$, $B$ and $t$ at various loading angles

| Angle/(°) | $\sigma_3$=5 MPa | | | $\sigma_3$=10 MPa | | |
|---|---|---|---|---|---|---|
| | $A$/GPa | $B$/GPa | $t$ | $A$/GPa | $B$/GPa | $t$ |
| 0 | 3.343 | 7.963 | 0.065 2 | 3.295 | 7.631 | 0.065 9 |
| 15 | 2.947 | 7.895 | 0.062 4 | 3.057 | 7.100 | 0.068 7 |
| 30 | 2.559 | 7.391 | 0.083 9 | 2.965 | 6.734 | 0.070 7 |
| 45 | 2.354 | 7.353 | 0.088 6 | 2.472 | 6.487 | 0.074 3 |
| 60 | 2.608 | 7.412 | 0.089 4 | 3.196 | 6.875 | 0.069 9 |
| 90 | 2.917 | 7.509 | 0.073 1 | 3.805 | 7.270 | 0.057 8 |

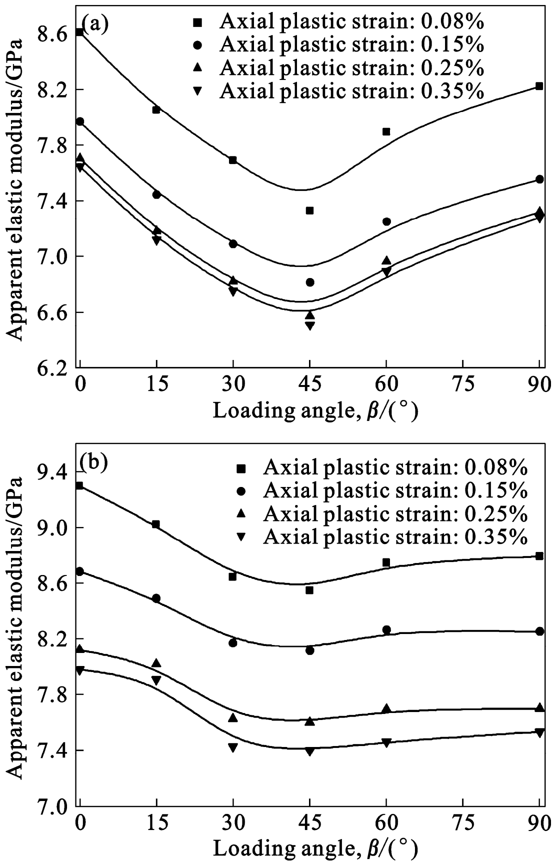


**Fig. 8** Contour curves for apparent elastic modulus vs loading angle at equivalent axial plastic strain: (a) $\sigma_3$=5 MPa; (b) $\sigma_3$=10 MPa

1) At the same values of $\varepsilon_a^p$, $E_\beta$ at 10 MPa confining pressure is greater than that under 5 MPa. This illustrates that higher confining pressure has a considerable effect on elastic modulus.

2) The anisotropy degree at 5 MPa confining pressure is more evident than that under 10 MPa. And it is clear that as the confining stress grows larger, the argillite anisotropy becomes weaker. Therefore, higher confining pressures can significantly restrain anisotropic deformation of rocks.

3) The degree of argillite anisotropy depends highly upon plastic internal variable. With the growth of axial plastic strain, apparent elastic modulus and the degree of argillite's anisotropy reduce.

Only apparent Poisson ratios for $\beta$=0°, 45° and 90° were obtained. With Eq. (6), $v_\beta$ can be calculated corresponding to each unloading cycle. It is significant to find that $v_\beta$ increases with the growth of $\varepsilon_a^p$ and it eventually tends to constant. Similarly, it is feasible to establish an empirical relation between $v_\beta$ and $\varepsilon_a^p$, which is

$$v_\beta = a - bc^{\varepsilon_a^p} \tag{13}$$

where $a$, $b$ and $c$ are the empirical parameters related to loading angles and confining pressures. Experimental values of $v_\beta$ vs $\varepsilon_a^p$ and data-fitting curves with Eq. (13) are shown in Fig. 9 at three loading angles and at two confining stresses of 5 MPa and 10 MPa. Three empirical parameters of Eq. (13) are listed in Table 4.

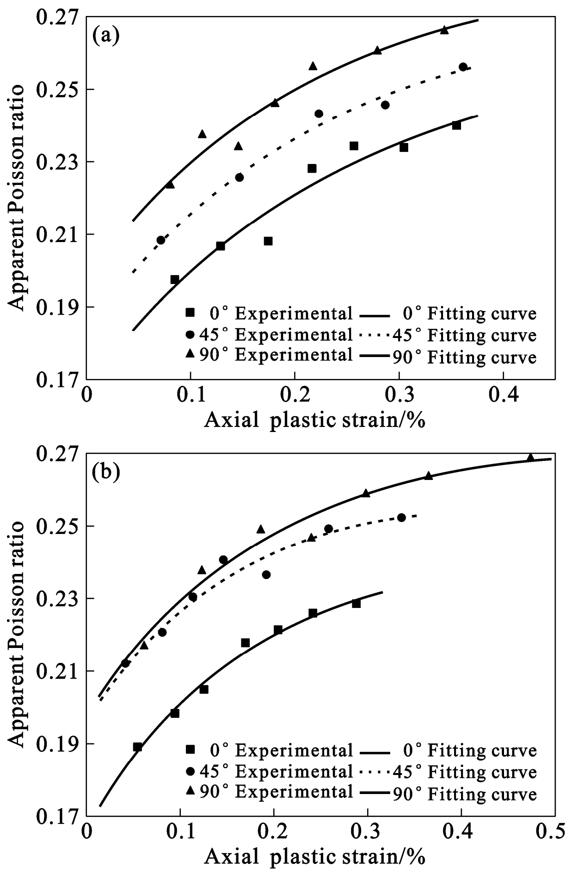


**Fig. 9** Relationships between apparent Poisson ratio and axial plastic strain at two confining pressures: (a) $\sigma_3$=5 MPa; (b) $\sigma_3$=10 MPa

**Table 4** Values of $a$, $b$ and $c$ at various loading angles

| Angle/(°) | $\sigma_3$=5 MPa | | | $\sigma_3$=10 MPa | | |
|---|---|---|---|---|---|---|
| | $a$ | $b$ | $c$ | $a$ | $b$ | $c$ |
| 0 | 0.264 | 0.096 0 | 0.017 93 | 0.244 | 0.077 9 | 0.002 73 |
| 45 | 0.272 | 0.089 4 | 0.010 21 | 0.258 | 0.062 6 | 0.001 03 |
| 90 | 0.284 | 0.086 4 | 0.009 14 | 0.274 | 0.076 9 | 0.004 71 |

In Eqs. (12) and (13), when $\varepsilon_a^p \to 0$, the values that $E_\beta$ and $\nu_\beta$ tend to be are defined as original values of apparent elastic modulus and apparent Poisson ratio and recorded as $E_\beta^0$ and $\nu_\beta^0$ correspondingly. As $E_\beta^0$ and $\nu_\beta^0$ are obtained (listed in Table 5), elastic strain and coupled elasto-plastic strain can be calculated by Eqs. (7) and (8). It is evident that $E_\beta^0$ and $\nu_\beta^0$ vary with loading angles.

**Table 5** Values of $E_\beta^0$, and $\nu_\beta^0$ at various loading angles

| $\beta$/(°) | 5 MPa | | 10 MPa | |
|---|---|---|---|---|
| | $E_\beta^0$/GPa | $\nu_\beta^0$ | $E_\beta^0$/GPa | $\nu_\beta^0$ |
| 0 | 10.93 | 0.17 | 11.31 | 0.17 |
| 15 | 10.16 | — | 10.84 | — |
| 30 | 9.70 | — | 9.95 | — |
| 45 | 8.96 | 0.18 | 9.71 | 0.20 |
| 60 | 10.07 | — | 10.02 | — |
| 90 | 11.08 | 0.20 | 10.43 | 0.20 |

### 4.2 Variations of five elastic parameters

Based on the testing methodology described in previous sections and provided in Refs. [1−2], the five elastic parameters for the test anisotropic argillite can be determined. Because of coupled elasto-plastic deformation, these five elastic parameters are related to plastic internal variable.

When $\beta$=0°, $E_\beta$=$E_2$ and $\nu_\beta$=$\nu_2$, and when $\beta$=90°, $E_\beta$=$E_1$ and $\nu_\beta$=$\nu_1$. From the anisotropic elastic theory, calculation procedure of $G_2$ can be presented as follows.

1) Let axial plastic strain $\varepsilon_a^p$ be a series of constant values $\xi_1$, $\xi_2$,⋯ $\xi_n$, Input this series of values into functions $E_1$=$E_2(\varepsilon_a^p)$, $E_2$=$E_2(\varepsilon_a^p)$, $E_\beta$=$E_\beta(\varepsilon_a^p)$, and $\nu_2=\nu_2(\varepsilon_a^p)$, and obtain a series of values for $E_1$, $E_2$, $E_\beta$ and $\nu_2$, corresponding to $\xi_1$, $\xi_2$, ⋯, $\xi_n$.

2) Input these values into Eqs. (13) and (14) in Ref. [1], then we obtain several series of values for $G_2$ corresponding to $\xi_1$, $\xi_2$, ⋯, $\xi_n$.

3) Use an exponential decay function (the same as Eq. (12)) to fit the relationship between $G_2$ and axial plastic strain $\varepsilon_a^p$.

The calculated values and data-fitting curves of $G_2$ vs $\varepsilon_a^p$ are shown in Fig. 10 at different confining pressures of 5 MPa and 10 MPa.

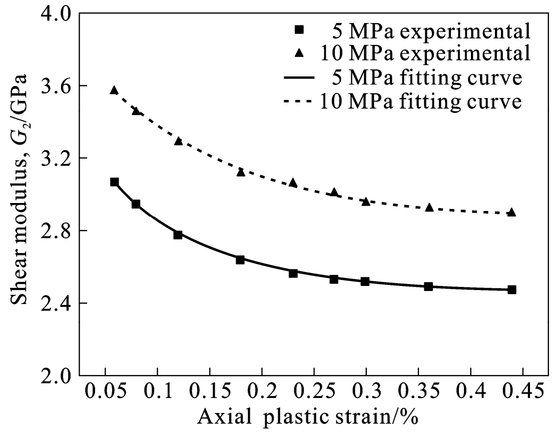


**Fig. 10** Relationships between shear modulus and plastic internal variables at two confining pressures

Significantly, based on these values, empirical functions between five elastic parameters of anisotropic argillite and axial plastic strain are obtained in the form of Eqs. (14) and (15) corresponding to 5 MPa and 10 MPa confining pressures, respectively:

$$\begin{cases} E_1 = 7.270 + 3.805\exp(-\dfrac{\varepsilon_a^p}{0.0578}) \\ E_2 = 7.631 + 3.295\exp(-\dfrac{\varepsilon_a^p}{0.065\ 9}) \\ G_2 = 2.469 + 1.143\exp(-\dfrac{\varepsilon_a^p}{0.0921}) \\ \nu_1 = 0.284 - 0.086\ 4 \times 0.009\ 14^{\varepsilon_a^p} \\ \nu_2 = 0.264 - 0.096\ 0 \times 0.017\ 93^{\varepsilon_a^p} \end{cases} \tag{14}$$

$$\begin{cases} E_1 = 7.509 + 2.917\exp(-\dfrac{\varepsilon_a^p}{0.073\ 1}) \\ E_2 = 7.963 + 3.343\exp(-\dfrac{\varepsilon_a^p}{0.065\ 2}) \\ G_2 = 2.868 + 1.123\exp(-\dfrac{\varepsilon_a^p}{0.122\ 6}) \\ \nu_1 = 0.274 - 0.076\ 9 \times 0.004\ 71^{\varepsilon_a^p} \\ \nu_2 = 0.244 - 0.077\ 9 \times 0.002\ 73^{\varepsilon_a^p} \end{cases} \tag{15}$$

## 5 Characteristics of coupled elasto-plastic deformation of anisotropic argillite

### 5.1 Relations between axial springback strain and plastic strain

For a better understanding of the characteristics of the anisotropic argillite's coupled elasto-plasticity, a comparison of deformational effect between coupled elasto-plasticity existing (E-P coupling) and no coupled elasto-plasticity existing (Non E-P coupling) is presented in the following. Before this discussion, two variables related to plastic strain are defined.

Firstly, taking into account the coupled elasto-plasticity, we define a ratio of axial reversible strain $\varepsilon_{\mathrm{a}}^{\mathrm{r}(i)}$ to the total strain increment $\Delta\varepsilon_{\mathrm{a}}^{(i)}$ during each cycle loading as

$$\lambda=\frac{C_iF_i}{C_{i-1}F_i}=\frac{\varepsilon_{\mathrm{a}}^{\mathrm{r}(i)}}{\Delta\varepsilon_{\mathrm{a}}^{(i)}} \tag{16}$$

Secondly, by contrast, assume that the argillite had no coupled elasto-plastic deformation. Another ratio in terms of axial elastic strain $\varepsilon_{\mathrm{a}}^{\mathrm{e}(i)}$ to the total strain increment $\Delta\varepsilon_{\mathrm{a}}^{(i)}$ during each loading cycle is defined as

$$\mu=\frac{H_iF_i}{C_{i-1}F_i}=\frac{\varepsilon_{\mathrm{a}}^{\mathrm{e}(i)}}{\Delta\varepsilon_{\mathrm{a}}^{(i)}} \tag{17}$$

Input the values of original apparent elastic modulus $E_\beta^0$ listed in Table 5 into Eq. (7), and values of $\varepsilon_{\mathrm{a}}^{\mathrm{e}(i)}$ can be obtained.

Obviously, we have $0<\lambda<1$ and $0<\mu<1$. This normalization approach is useful, because it can make it possible to compare quantitatively the elastic properties while loading strain increments are not equal. By tests and calculation, we can establish the relationships of $\lambda$ vs $\varepsilon_{\mathrm{a}}^{\mathrm{p}(i)}$ and $\mu$ vs $\varepsilon_{\mathrm{a}}^{\mathrm{p}(i)}$, which are in form of experimental values and data-fitting curves as illustrated in Figs. 11 and 12 at two confining pressures. Fitting functions are in a common form as

$$y=m-nd^x \tag{18}$$

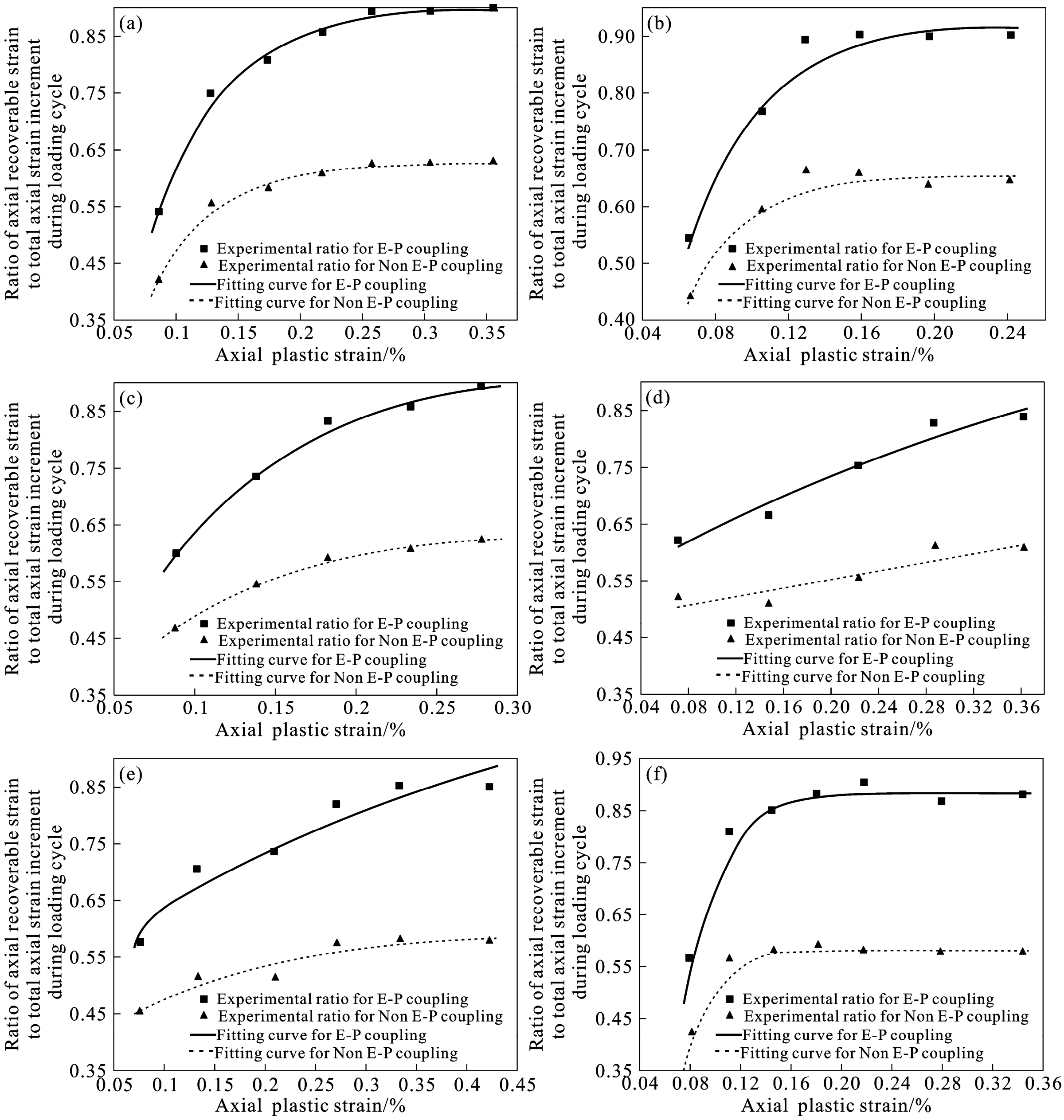


**Fig. 11** Relationships between $\lambda$ (or $\mu$) and $\varepsilon_{\mathrm{a}}^{\mathrm{p}}$ under different loading angles $\beta$ (confining pressure: 5 MPa): (a) 0°; (b) 15°; (c) 30°; (d) 30°; (e) 60°; (f) 90°

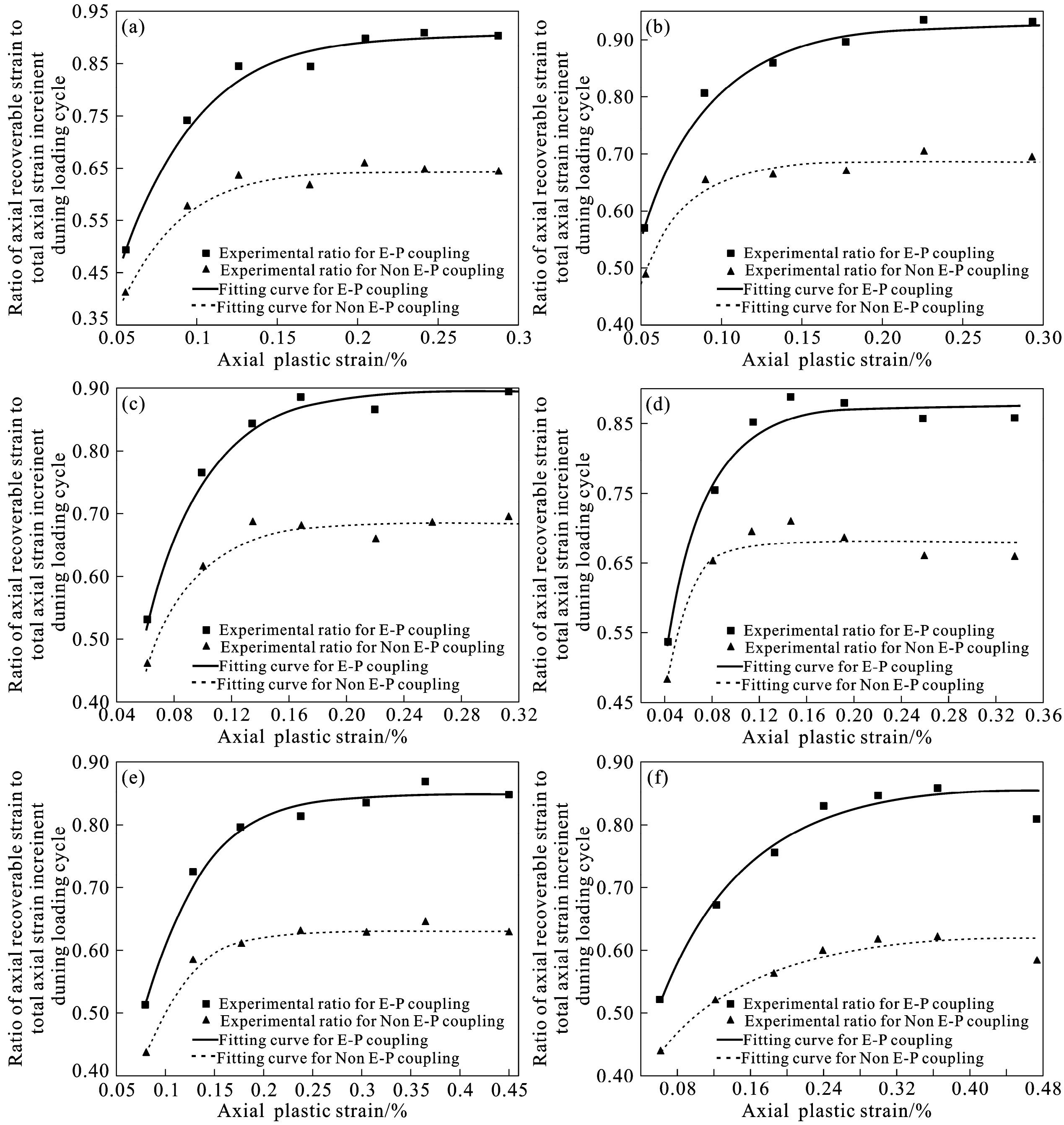


**Fig. 12** Relationships between $\lambda$ (or $\mu$) and $\varepsilon_{\mathrm{a}}^{\mathrm{p}}$ under different loading angles $\beta$ (confining pressure: 10 MPa) : (a) 0°; (b) 15°; (c) 30°; (d) 30°; (e) 60°; (f) 90°

where $y$ represents $\lambda$ or $\mu$, and $x$ refers to axial plastic strain $\varepsilon_{\mathrm{a}}^{\mathrm{p}}$. $m$, $n$ and $d$ are empirical parameters used in data fitting and related to loading angles and confining pressures.

From Figs. 11 and 12, $\lambda$ and $\mu$ increase with the growth of $\varepsilon_{\mathrm{a}}^{\mathrm{p}}$. When $\varepsilon_{\mathrm{a}}^{\mathrm{p}}$ is low, the increase amplitudes of $\lambda$ and $\mu$ are considerably large. With the growth of $\varepsilon_{\mathrm{a}}^{\mathrm{p}}$, curves tend to stable values. It is noteworthy that $\mu<\lambda$, and with the growth of plastic strain $\varepsilon_{\mathrm{a}}^{\mathrm{p}}$, the gaps between them increase.

## 5.2 Anisotropy of argillite in coupled elasto-plastic deformation

A good way to study the argillite's anisotropic coupled elasto-plastic deformational charaterisitcs is to graph the contour curves of $\lambda$ vs $\beta$ at equivalent axial plastic strain $\varepsilon_{a}^{p}$.

According to the test results, at 5 MPa confining pressure, we set $x$=0.08%, 0.15%, 0.25% and 0.35%. At 10 MPa, however, set $x$=0.06%, 0.10%, 0.20% and 0.35%. Here, $x$ refers to axial plastic strain $\varepsilon_{\mathrm{a}}^{\mathrm{p}}$. Firstly, let $\beta$=0°, input these four values of $x$ into Eq. (18) and four different values of $y$ ($y=\lambda$) are obtained. Through the same calculating processes, another five sets of values of $\lambda$ corresponding to $\beta$=15°, 30°, 45°, 60° and 90° are obtained. Link the points of $\lambda$ with same value of $\varepsilon_a^p$ by line segments to be curves, which are the contour curves of $\lambda$ vs $\beta$ at equivalent $\varepsilon_a^p$ (Fig. 13). From these curves, two main characteristics can be observed:

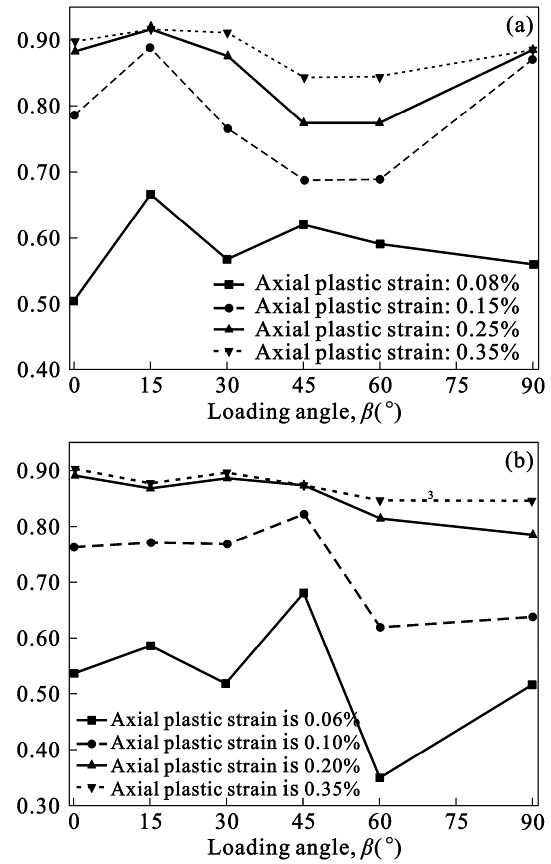


**Fig. 13** Anisotropy of coupled elasto-plasticity for tested argillite–contour curves of $\lambda$ vs $\beta$ at $\varepsilon_a^p$: (a) $\sigma_3$=5 MPa; (b) $\sigma_3$=10 MPa

1) At low plastic strain phase, argillite has a high anisotropic degree in coupled elasto-plastic deformation. With the growth of plastic strain, the degree of anisotropy reduces and the variation of $\lambda$ with $\beta$ tends to be gentle.

2) Confining pressure has a salient influence on the anisotropic degree of argillite's coupled elasto-plastic deformation. As plastic strain and confining pressure increase, anisotropic degree of this kind of deformation is suppressed.

## 6 Conclusions

1) Based on a review of previous works about rocks' coupled elasto-plasticity, a caption on this issue is illustrated graphically. More practically, a kind of bedding argillite (which is of transverse isotropy) is selected to conduct triaxial cyclic loading tests.

2) On the loading process, argillite's mechanical response is of elasto-plasticity and the moduli determined by loading curves are less than those tested by unloading curves, of which can better reflect argillite's elastic properties to a large extent. So, elastic parameters of argillite are measured by unloading curves.

3) The apparent elastic modulus of tested argillite at 10 MPa confining pressure is larger than that at the confining pressure of 5 MPa at the same loading angle. It means that higher confining pressure has a positive effect on argillite's elastic properties.

4) With the growth of axial plastic strain, the bedding argillite's apparent elastic modulus decreases in a form of exponential decay function, whereas apparent Poisson ratio increase is in the form of power equation. The degradation of elastic parameters induced by coupled elasto-plasticity accords well with the previous research results.

5) Anisotropic effect of tested argillite's coupled elasto-plasticity has been investigated by discussing the shape of contour curves of $E_\beta$ vs $\beta$ and of $\lambda$ vs $\beta$ at equivalent $\varepsilon_a^p$ at two confining pressures. It has been found that the anisotropic degree of bedding argillite is suppressed with the growth of confining pressures and axial plastic strains. This indicates that higher confining pressure and larger accumulated plastic strains have strong inhibitions upon the argillite's anisotropy in deformation.

6) A reinforcement effect on elastic parameters is observed, which is related to restraint effect of higher confining pressure. A comparison, between the curves of $\lambda$ vs $\varepsilon_a^p$ and $\mu$ vs $\varepsilon_a^p$ provides a striking illustration that transversely isotropic argillite has a conspicuous coupled elasto-plastic deformation, because much more reversible strains are included in the total strain increment in subsequent loading cycles. So, anisotropy and coupled elasto-plasticity upon the elastic parameters are essentially required in the elaborate description of mechanical properties of the anisotropic argillite.

## References

[1] AMADEI B. Importance of anisotropy when estimating and measuring in situ stresses in rock [J]. International Journal of Rock Mechanics and Mining Sciences & Geomechanics Abstracts, 1996, 33(3): 293−325.

[2] HAKALA M, KUULA H, HUDSON J A. Estimating the transversely isotropic elastic intact rock properties for in situ stress measurement data reduction: A case study of the Olkiluoto Mica Gneiss, Finland [J]. International Journal of Rock Mechanics and Mining Sciences, 2007,

44(1): 14−46.

[3] NASSERI M H B, RAO K S, RAMAMURTHY T. Anisotropic strength and deformational behavior of Himalayan Schists [J]. International Journal of Rock Mechanics and Mining Sciences, 2003, 40(1): 3−23.

[4] NUNES A L L S. A new method for determination of transverse isotropic orientation and the associated elastic parameters for intact rock [J]. International Journal of Rock Mechanics and Mining Sciences, 2002, 39(2): 257−273.

[5] OLSSON W A. Development of anisotropy in the incremental shear moduli for rock undergoing inelastic deformation [J]. Mechanics of Materials, 1995, 21(3): 231−242.

[6] BIGONI D, HUECKEL T. Uniqueness and localization—I. Associative and non-associative elastoplasticity [J]. International Journal of Solids and Structures, 1991, 28(2): 197−213.

[7] BIGONI D, HUECKEL T. Uniqueness and localization—II. Coupled elastoplasticity [J]. International Journal of Solids and Structures, 1991, 28(2): 215−224.

[8] DAFALIAS Y F. Il'iushin's postulate and resulting thermodynamic conditions on elasto-plastic coupling [J]. International Journal of Solids and Structures, 1977, 13(3): 239−251.

[9] DAFALIAS Y F. Elasto-plastic coupling within a thermodynamic strain space formulation of plasticity [J]. International Journal of Non-Linear Mechanics, 1977, 12(5): 327−337.

[10] MAIER G, HUECKEL T. Nonassociated and coupled flow rules of elastoplasticity for rock-like materials [J]. International Journal of Rock Mechanics and Mining Sciences &; Geomechanics Abstracts, 1979, 16(2): 77−92.

[11] GONZAGA G G, LEITE M H, CORTHÉSY R. Determination of anisotropic deformability parameters from a single standard rock specimen [J]. International Journal of Rock Mechanics and Mining Sciences, 2008, 45(8): 1420−1438.

[12] TALESNICK M L, BLOCH-FRIEDMAN E A. Compatibility of different methodologies for the determination of elastic parameters of intact anisotropic rocks [J]. International Journal of Rock Mechanics and Mining Sciences, 1999, 36(7): 919−940.

[13] TALESNICK M L, RINGEL M. Completing the hollow cylinder methodology for testing of transversely isotropic rocks: torsion testing [J]. International Journal of Rock Mechanics and Mining Sciences, 1999, 36(5): 627−639.

[14] DUVEAU G, SHAO J F. A modified single plane of weakness theory for the failure of highly stratified rocks [J]. International Journal of Rock Mechanics and Mining Sciences, 1998, 35(6): 807−813.

[15] GAO Z, ZHAO J, YAO Y. A generalized anisotropic failure criterion for geomaterials [J]. International Journal of Solids and Structures, 2010, 47(22/23): 3166−3185.

[16] LADE P V. Modeling failure in cross-anisotropic frictional materials [J]. International Journal of Solids and Structures, 2007, 44(16): 5146−5162.

[17] LU Guang-yin, ZHU Zi-qiang, LIU Qun-yi, He Xian-qi. Failure mode and strength anisotropic characteristic of stratified rock mass under uniaxial compressive situation [J]. Journal of Central South University of Technology, 2009, 16(4): 663−668.

[18] PIETRUSZCZAK S, MROZ Z. Formulation of anisotropic failure criteria incorporating a microstructure tensor [J]. Computers and Geotechnics, 2000, 26(2): 105−112.

[19] TIEN Y M, KUO M C. A failure criterion for transversely isotropic rocks [J]. International Journal of Rock Mechanics and Mining Sciences, 2001, 38(3): 399−412.

[20] PIETRUSZCZAK S, LYDZBA D, SHAO J F. Modelling of inherent anisotropy in sedimentary rocks [J]. International Journal of Solids and Structures, 2002, 39(3): 637−648.

[21] CHEN L, SHAO J F, HUANG H W. Coupled elastoplastic damage modeling of anisotropic rocks [J]. Computers and Geotechnics, 2010, 37(1/2): 187−194.

[22] CHEN L, SHAO J F, ZHU Q Z, DUVEAU G. Induced anisotropic damage and plasticity in initially anisotropic sedimentary rocks [J]. International Journal of Rock Mechanics and Mining Sciences, 2012, 51(4): 13−23.

[23] Zhu Q Z, ZHOU C B, SHAO J F, KONDO. A discrete thermodynamic approach for anisotropic plastic-damage modeling of cohesive-frictional geomaterials [J]. Int J Numer Anal Methods Geomech, 2010, 34(12): 1250−1270.

[24] ZHU W, WALSH J B. A new model for analyzing the effect of fractures on triaxial deformation [J]. International Journal of Rock Mechanics and Mining Sciences, 2006, 43(8): 1241−1255.

[25] VOYIADJIS G Z. Degradation of elastic modulus in elastoplastic coupling with finite strains [J]. International Journal of Plasticity, 1988, 4(4): 335−353.

[26] YOSHINAKA R, TRAN T V, OSADA M. Pore pressure changes and strength mobilization of soft rocks in consolidated-undrained cyclic loading triaxial tests [J]. International Journal of Rock Mechanics and Mining Sciences, 1997, 34(5): 715−726.

[27] YOSHINAKA R, TRAN T V, OSADA M. Non-linear, stress- and strain-dependent behavior of soft rocks under cyclic triaxial conditions [J]. International Journal of Rock Mechanics and Mining Sciences, 1998, 35(7): 941−955.

[28] FUENKAJORN K, PHUEAKPHUM D. Effects of cyclic loading on mechanical properties of Maha Sarakham salt [J]. Engineering Geology, 2010, 112(1/2/3/4): 43−52.

[29] HEAP M J, FAULKNER D R. Quantifying the evolution of static elastic properties as crystalline rock approaches failure [J]. International Journal of Rock Mechanics and Mining Sciences, 2008, 45(4): 564−573.

[30] ZHANG Kai, ZHOU Hui, FENG Xia-ting, SHAO Jian-fu. Experimental research on elastoplastic coupling character of marble [J]. Rock and Soil Mechanics, 2010, 31(8): 2425−2434. (in Chinese).

[31] NIANDOU H, SHAO J F, HENRY J P. Laboratory investigation of the mechanical behaviour of Tournemire shale [J]. International Journal of Rock Mechanics and Mining Sciences, 1997, 34(1): 3−16.

[32] ZHANG Jiu-chang, PENG Li, XU Xiang-hua, ZHU Neng-wen. Experimental study of elastoplastic coupling deformation for transversely isotropic rocks [J]. Chinese Journal of Rock Mechanics and Engineering, 2011, 30(2): 267−274. (in Chinese).

**(Edited by DENG Lü-xiang)**